Hyperfine Structure of the $B\ ^2\Sigma \rightarrow X\ ^2\Sigma$ Transition of the LaO Molecule

R. Bacis and R. Collomb

Laboratoire de Spectrométrie Ionique et Moléculaire, Associé au Centre National de la Recherche Scientifique, 43, Boulevard du 11 Novembre 1918, 69621-Villeurbanne, France

N. Bessis

Laboratoire de Spectroscopie et de Luminescence, 43, Boulevard du 11 Novembre 1918, 69621-Villeurbanne, France

(Received 1 May 1973)

The O-O band of the $B\ ^2\Sigma \rightarrow X\ ^2\Sigma$ transition of lanthanum oxide has been studied using an interference spectrometer HYPEAC and a "dressed-walls" hollow cathode. The accuracy of the measurements allows a detailed study of nuclear hyperfine effects. A theoretical interpretation of experimental results is proposed which takes into account residual fine- and hyperfine-interaction contributions. A satisfactory explanation of the variation with N of the intensities is obtained when introducing intermediate coupling b_{β_s}-b_{β_l} effects in the ground state. From the comparison between experimental and theoretical results, the following values of some hyperfine- and fine-structure parameters are deduced, i.e., for the $X\ ^2\Sigma$ state $\gamma_{SR} = 2.57 \pm 0.25$ mK and $b = 123.5 \pm 1.8$ mK, and for the $B\ ^2\Sigma$ state $b' = 21.7 \pm 2.0$ mK and $c' = -5 \pm 12$ mK.

I. INTRODUCTION

Analysis of the electronic spectrum of some rare-earth molecules has shown a doubling of many rotational lines corresponding to a two-level splitting of the lower state. This doubling has been observed for the LaO,[1-3] ScO,[4-7] LaS,[8] LuO[9-11] molecules and is now interpreted in terms of strong magnetic hyperfine interactions in the ground state.[12-16] Accurate spectrographic measurements led, for the ScO[6] molecule to a constant value, i.e., (257 ± 1) mK of this two-level interval, while Green,[3] when he investigated the $C\ ^2\Pi \rightarrow X\ ^2\Sigma$ transition of the LaO molecule, pointed out a slight variation of this splitting with N'', i.e., $(484 \pm 0.34\,N'')$ mK. Using a Fabry-Perot spectrometer, it is possible to carry out a much more accurate experimental study of the LaO $B\ ^2\Sigma \rightarrow X\ ^2\Sigma$ transition (O-O band). Complex variations of this splitting are observed which cannot be explained only by assuming an $X\ ^2\Sigma$ hyperfine isotropic structure. Moreover, our experimental setup enables the determination of the line shapes and, particularly, the measures of their half-widths.

In Sec. II of this paper, the main experimental results are summed up; the corresponding theoretical interpretation is given in Sec. III. From the comparison of experimental and theoretical results, it has been possible to deduce the values or the order of magnitude of some of the fine and hyperfine structure parameters of the two states.

II. EXPERIMENTAL

A. Apparatus

The walls of the source, a hollow-cathode lamp, are "dressed" with different alloys: La-La_2O_3, 3Cu-La_2O_3, or 3Ag-La_2O_3.[17] It works with a double anode and an additional discharge. Thus, for a given linewidth, we gain a factor of 100 on the signal intensity with respect to a classical lamp (La_2O_3 powder put down in the cathodic hole).[18]

The $B\ ^2\Sigma \rightarrow X\ ^2\Sigma$ (O-O) band lies between 5600 and 5625 Å. It has been studied with the help of an interference spectrometer HYPEAC,[19] in order to obtain a best precision. Its grating spectrometer is scanned in synchronism with one Fabry-Perot interferometer. A pressure variation of 2 atm gives a scanning interval of about 10 000 mK.[17] The centers of gravity of the lines are determined with respect to the fringes of a second Fabry-Perot, which are calibrated in comparison with interferometrically measured thorium lines[20] emitted in a hollow cathode cooled with liquid nitrogen. By taking due precautions, these measures are as accurate as those of the proposed secondary standards (thorium wavelengths). Moreover, this reference source enables us to obtain the instrumental profile of the spectrometer.[21]

The recordings have been performed with the help of a Fabry-Perot of 7.5 mm thickness, and the real resolution $\nu/\Delta\nu$ is better than 800 000, when the reference source works at very low current (a few milliamperes). The LaO spectrum has been recorded at different intensities (from 25 to about 100 mA). In the former case, the resolution is 500 000 for the lines with negligible hyperfine broadening. Principally, the P branches have been measured, the R branches determination being more difficult because of their returning. Some lines of the spectrum are presented on Fig. 1 together with reference fringes.

At 25 mA the overlapping of the P branches by

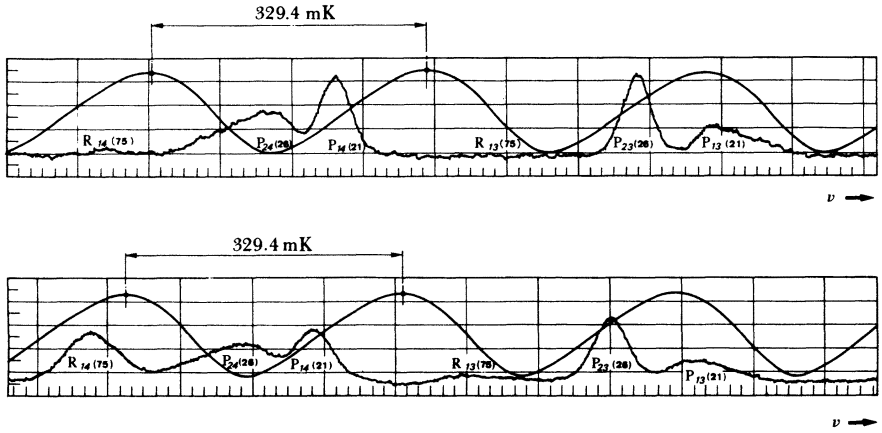

FIG. 1. (a) Liquid-nitrogen-cooled dressed-walls hollow cathode, $I = 50$ mA; (b) water-cooled dressed-walls hollow cathode, $I = 300$ mA.

the R branches is greatly reduced, and a precise determination of linewidths and intervals may be carried out down to the proximity of the zero gap.

Finally, in order to build up a rotational line, one has to know the shape of a hyperfine component. For this purpose, lines having a minimum width and belonging to the P_{14} [Fig. 2(b)] and P_{23} branches [Fig. 2(c)] are measured point by point on the recordings, as their hyperfine broadening is weak. Indeed, we have checked that the real resolution corresponding to these lines increases normally as compared to the thorium lines, when the current is lowered (for 10 mA, a value of $R \sim 600\,000$ is reached).

Moreover, when the instrumental profile is taken into account, the comparison of the corresponding Doppler temperatures of these lines with those deduced from the linewidths of La and Ar, confirms the small hyperfine broadening. The validity of this fact will be verified during the theoretical setting up of the line shapes.

B. Results

The main feature of the electronic spectrum of LaO is the appearance of doublets, the spacing of which varies weakly with the different lines of the P_1 ($J' = N' + \frac{1}{2}$) and P_2 ($J' = N' - \frac{1}{2}$) branches. These lines are observed in a region of weak overlapping ($N < 50$). The distance between the two P_1 components increases with N, while in the case of the P_2 components, it decreases (Fig. 3).

The characteristic forms of the lines are shown in Fig. 1. For N greater than 10, the components P_{23} and P_{14} are practically symmetric and relatively sharp; their widths present a minimum at $N \simeq 35$. For $N < 10$, shapes and distances vary in a complex way. The P_{24} and P_{13} components are asymmetrical and large and their widths increase with N [Figs. 2(d) and 2(a)]. It should be noted that for the R-branch lines, a similar variation has been observed.

We also note that the ratio ρ_1 ($= P_{14}$ intensity/P_{13} intensity) increases with N; the same increase is also observed for the R branches [see for instance the line $R_1(75)$ in Fig. 1(b) where the R_1 branch is more intense because of the higher temperature of the source]. On the other hand, the ratio ρ_2 ($= P_{24}$ intensity/P_{23} intensity) decreases with N (Fig. 4). A qualitative explanation of this variation will be given further.

Besides, the distances between the lines of the P_1 and P_2 branches, related to the same value of N, increase with this quantum number owing to the great value of the γ' constant (~450 mK). This fact involves a large spin-orbit interaction in the $B^2\Sigma$ state, which will be studied in a forthcoming paper.

III. THEORETICAL

A. General Considerations

Our starting assumption has been already pointed out by different authors.[14,22-24] The spectrum of LaO (Fig. 5) shows general features related principally to the free-ion La^{++} spectrum. It is possible to assume that the ground $X^2\Sigma$ and the lowest-excited $A^2\Pi$ and $B^2\Sigma$ terms are substantially made up of a single unpaired electron centered on the metallic ion La^{++}. The corresponding orbitals involved are predominantly of s and p type and should be denoted later, respectively, $s\sigma$, $p\pi$, and $p\sigma$. Particularly, this starting point is in agreement with the well-known result[14] that the $A^2\Pi$ and $B^2\Sigma$ states are good examples of two states in pure precession.

In the $B^2\Sigma$ state the fine structure predominates over the hyperfine structure, and this state is a good case of almost pure b_{β_J} coupling ($\vec{J}' = \vec{N}' + \vec{S}$). The two-level splitting of this state ($J' = N' + \frac{1}{2}$ and $J' = N' - \frac{1}{2}$, noted, respectively, 1 and 2) arises principally from second-order electronic spin-orbit and rotational interactions with the $A^2\Pi$ states and obeys the well-known spin-splitting

rule[25] $\Delta = \gamma'(N' + \frac{1}{2})$.

In the $X^2\Sigma$ ground state the hyperfine structure is larger than the fine structure and arises almost entirely from the isotropic part, i.e., the Fermi contact term of the hyperfine interaction. Then, this state is a good case of b_{β_s} coupling; the nuclear spin $\vec{I}$ and electronic spin $\vec{S}$ are coupled together to give the resultant $\vec{G} = \vec{I} + \vec{S}$. The energy of each G level is

$$W_G = \tfrac{1}{2}b[G(G+1) - S(S+1) - I(I+1)], \quad (1)$$

where, within the single-electron approximation,

$$b = \tfrac{8}{3}\pi\zeta\langle S\sigma|\delta(\vec{r})|S\sigma\rangle,$$

with $\zeta = gg_I\mu_B\mu_N$; μ_B is the Bohr magneton, $g_I\mu_N$ is the dipolar magnetic nuclear moment, and $\delta(\vec{r})$

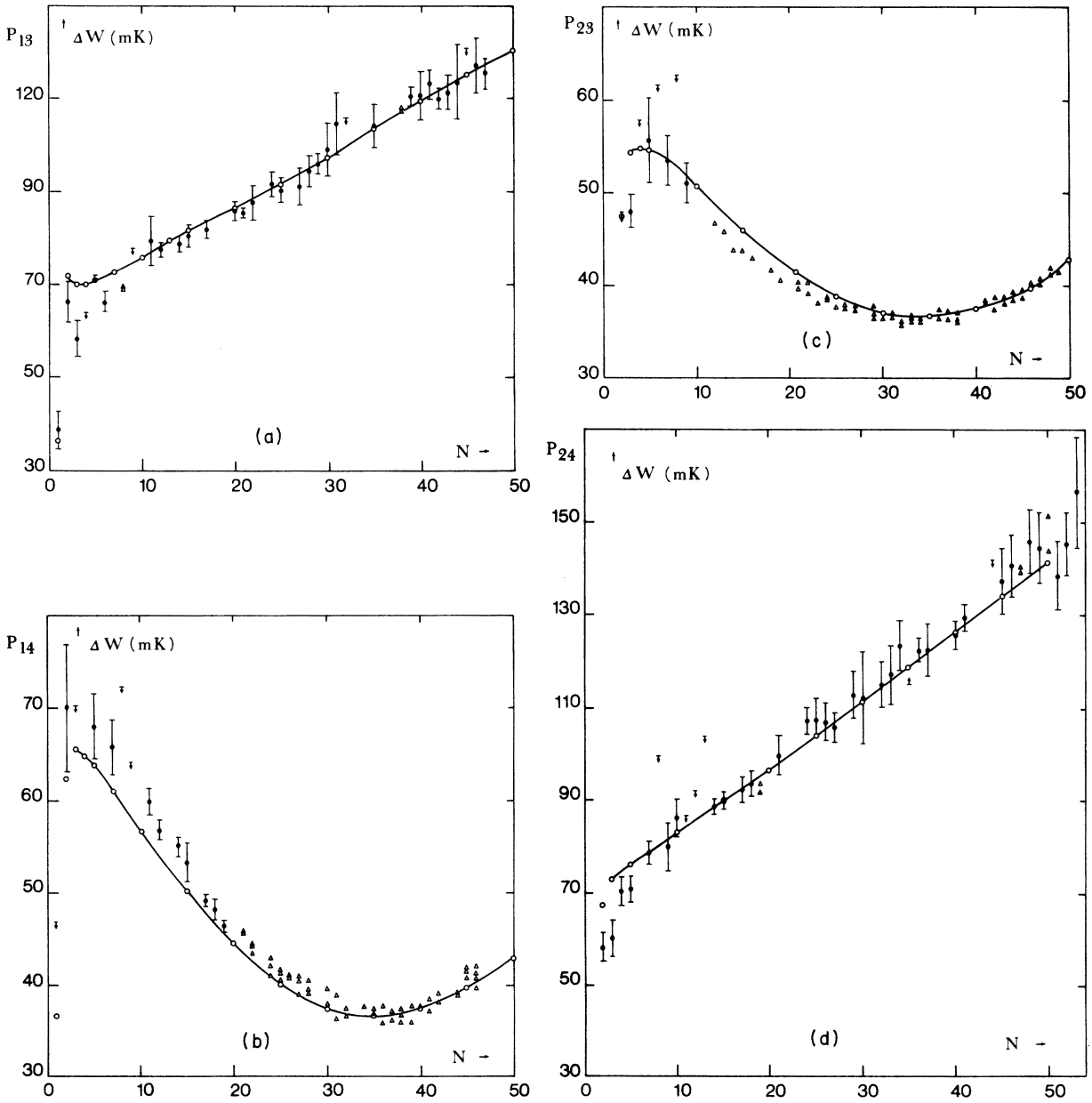

FIG. 2. Half-width ΔW of LaO lines. Δ, Experimental point; the vertical bar with a point at its center and short horizontal bars at each end are experimental points corresponding to the average of five measures or more (half-height = rms error between measures); vertical arrows pointing downwards with a short horizontal bar at the top give the maximum half-width for superposed lines; ○, theoretical values (which are joined by a solid line).

is the Dirac δ function. For La^{139} $g_I = 2.778$ nm.[26]

For $S = \frac{1}{2}$ and $I = \frac{7}{2}$ one gets the following expressions of the energies for the two-level splitting of this state ($G = 3$ and $G = 4$, noted, respectively, 3 and 4):

$$W_{G=3} = -\tfrac{9}{4}b\,, \quad W_{G=4} = \tfrac{7}{4}b\,, \quad W_{G=4} - W_{G=3} = 4b.$$

The observed branches correspond to $\Delta N = -1$ (P branches) and $\Delta N = +1$ (R branches). As it will be seen later, the intensity of the Q branches ($\Delta N = 0$) vanishes.

B. Pure Coupling Calculations

We first investigate the splitting of the principal levels by taking into account interaction terms of the Hamiltonian which have been neglected in Sec. III A. When introducing the hyperfine term of the Hamiltonian, each J' level in the $B^2\Sigma$ state is split into $2I+1$ sublevels F' ($\vec{F}' = \vec{J}' + \vec{I}'$). Likewise, when fine-structure interactions are considered, each G level of the $X^2\Sigma$ state gives rise to $(2G+1)$ sublevels $F(\vec{F} = \vec{N} + \vec{G})$. In fact, the principal branches observed result from the superposition of transitions between the F sublevels of the two states. In order to explain the experimental results, we have to calculate the corresponding transitions and their intensities.

1. *Sublevel Structure*

When introducing the Fermi-contact, magnetic dipole-dipole, and electric quadrupole terms of the hyperfine Hamiltonian, one obtains, for each principal J level of the $B^2\Sigma$ states ($J' = N' \pm \frac{1}{2}$) the following energies of the F' sublevels [Eq. (A3) of the Appendix]:

$$W'_{\text{Fermi}} = \frac{8\pi}{3}\zeta\frac{1}{4}\left(\frac{N'(N'+1) - J'(J'+1) - S(S+1)}{J'(J'+1)}\right) \times [F'(F'+1) - J'(J'+1) - I(I+1)]\langle p\sigma|\delta|p\sigma\rangle\,,$$

$$W'_{\text{dip-dip}} = \zeta\frac{(J'-\frac{1}{2})}{2J'(2J'+2)}[F'(F'+1) - J'(J'+1) - I(I+1)]\langle p\sigma|\frac{C_0^2}{r^3}|p\sigma\rangle\,,$$

$$W'_{\text{quad}} = \frac{e^2Q}{21}\left(\frac{\frac{3}{4}x(x-1) - I(I+1) - J'(J'+1)}{2J'(2J'+2)}\right)\langle p\sigma|\frac{C_0^2}{r^3}|p\sigma\rangle\,,$$

where $x = J'(J'+1) + I(I+1) - F'(F'+1)$ and C_0^2 is a second-rank orbital tensor. Q is the nuclear electric quadrupole moment. For La^{139}, $Q = 0.22 \times 10^{-24}$ cm^2.[27]

Within the single-electron scheme, the effective constants of the dipole-dipole and quadrupole terms include the same electronic integral; i.e., $\langle p\sigma|C_0^2/r^3|p\sigma\rangle$. So it is possible to express the excited energy levels in terms of only two unknowns. Considering only the F' dependency, we have

$$W'_{F'}(J' = N' + \tfrac{1}{2}) = \frac{1}{2}\left(b' + \frac{C'}{2N'+3}\right)\frac{F'(F'+1)}{2N'+1} + KC'\frac{x(x-1)}{(2N'+1)(2N'+3)}, \tag{2}$$

$$W'_{F'}(J' = N' - \tfrac{1}{2}) = \frac{1}{2}\left(-b' + \frac{C'}{2N'-1}\right)\frac{F'(F'+1)}{2N'+1} + KC'\frac{x(x-1)}{(2N'-1)(2N'+1)}, \tag{3}$$

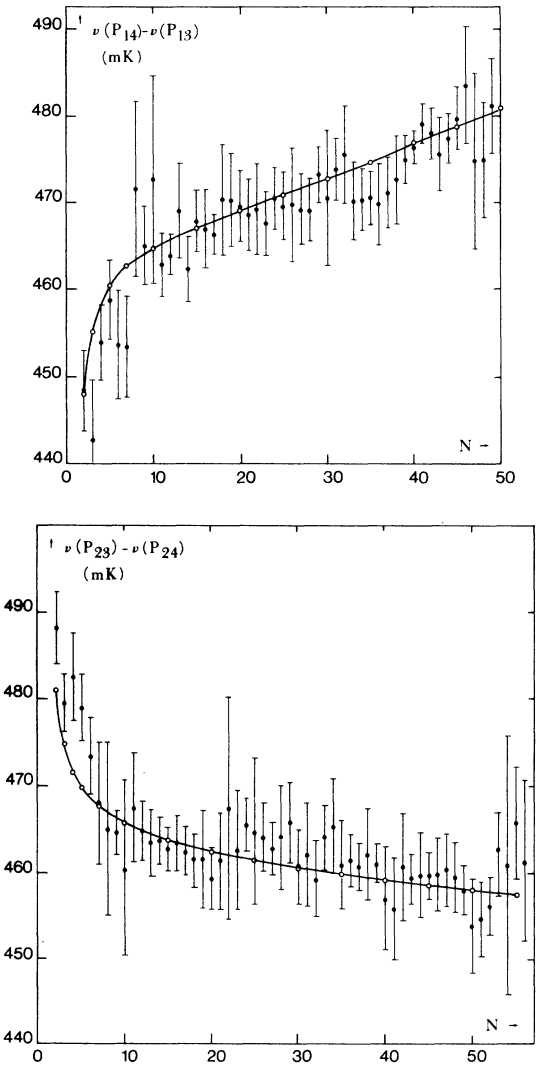

FIG. 3. Distance between centers of gravity. The vertical bar with a point at its center and short horizontal bars at each end are experimental points corresponding to the average of five measures or more (half-height = rms error between measures); ○, theoretical values (which are joined by a solid line).

where[28]

$$b' = \frac{8\pi}{3}\zeta\langle p\sigma|\delta|p\sigma\rangle + \zeta\langle p\sigma|\frac{C_0^2}{r^3}|p\sigma\rangle,$$

$$C' = -3\zeta\langle p\sigma|\frac{C_0^2}{r^3}|p\sigma\rangle,$$

$$K = -\frac{e^2Q}{84\zeta} = -0.008.$$

When taking into account the diagonal part of the electronic spin–nuclear rotation interaction, one obtains the following sublevel energies of the $X^2\Sigma$ state [Eq. (A2) of the Appendix]:

$$W_{G=4}(F) = \tfrac{7}{4}b + \tfrac{1}{16}\gamma_{SR}[F(F+1) - N(N+1) - G(G+1)], \quad (4)$$

$$W_{G=3}(F) = -\tfrac{9}{4}b - \tfrac{1}{16}\gamma_{SR}[F(F+1) - N(N+1) - G(G+1)]. \quad (5)$$

Within the single-unpaired-s-orbital approximation for the $X^2\Sigma$ state, residual hyperfine contributions, i.e., dipole-dipole and quadrupolar terms as well as second-order fine-structure interaction with the $^2\Pi$ states, are supposed to be small and have not been considered. It should be noted that for both $B^2\Sigma$ and $X^2\Sigma$ states, $\Lambda = 0$ and the orbital hyperfine term do not contribute. The nuclear spin–rotation interaction is neglected.

2. *Intensities*

From the relationships corresponding to a transition $b_{\beta_J} \rightarrow b_{\beta_S}$, we get the general expression [Eq. (B3) of the Appendix]

$$I(J'F' \rightarrow GF) = I_{FF'} = I_0(N, N')(2F+1)(2F'+1)\begin{Bmatrix} N' & F' & G \\ N & F & 1 \end{Bmatrix}^2 (2J'+1)(2G+1)\begin{Bmatrix} N' & S' & J' \\ I & F' & G \end{Bmatrix}^2, \quad (6)$$

where

$$\begin{Bmatrix} j_1 & j_2 & j_3 \\ l_1 & l_2 & l_3 \end{Bmatrix}$$

are Wigner "6j" coefficients and $I_0(N, N')$ does not depend on F, F', G, and J.

Using expressions of the energy levels [Eqs. (2)–(5)] and of the corresponding intensities [Eq. (6)] the theoretical positions of the centers of gravity of each lines are obtained:

$$W(J' \rightarrow G) = \sum_{F'F} I_{F'F}(W'_{F'} - W_F) \Big/ \sum_{F'F} I_{F'F}.$$

Consequently, the theoretical distances $W_{(J'\rightarrow G=4)} - W_{(J'\rightarrow G=3)}$ are finally expressed in terms of the parameters b, b', c', γ_{SR}. As the values of these distances are known from the experimental data for N varying from 1 to 50, one obtains an overdetermined linear system in these parameters, which can be solved by a least-squares adjustment. In fact, difficulties of compatibility for small and great values of N allow only the determination of

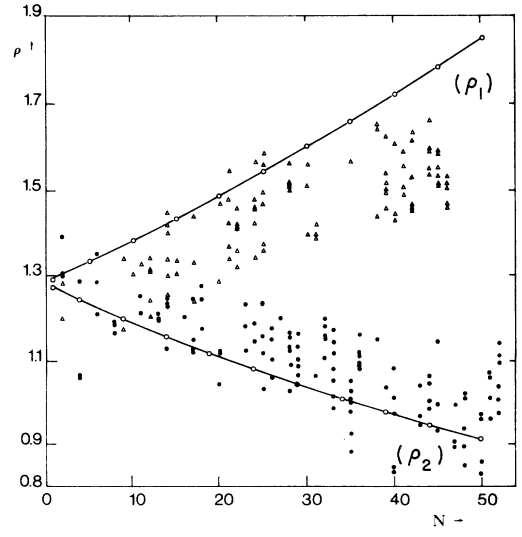

FIG. 4. △, P_{14} intensity/P_{13} intensity$=\rho_1$, ●, P_{24} intensity/P_{23} intensity$=\rho_2$, ○, theoretical values (which are joined by a solid line).

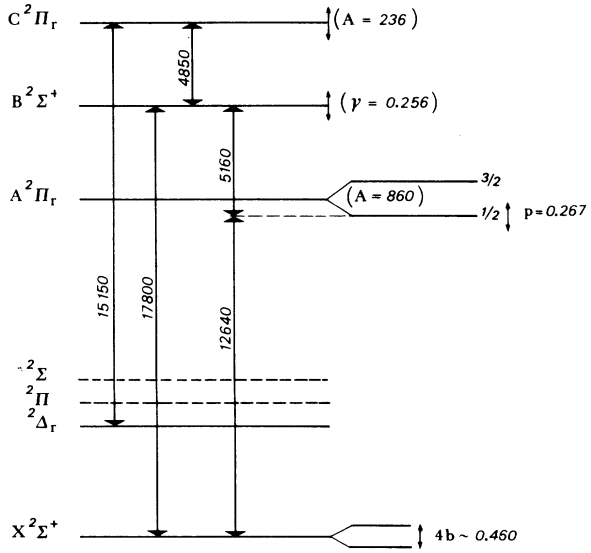

FIG. 5. Principal electronic levels of LaO (cm^{-1}).

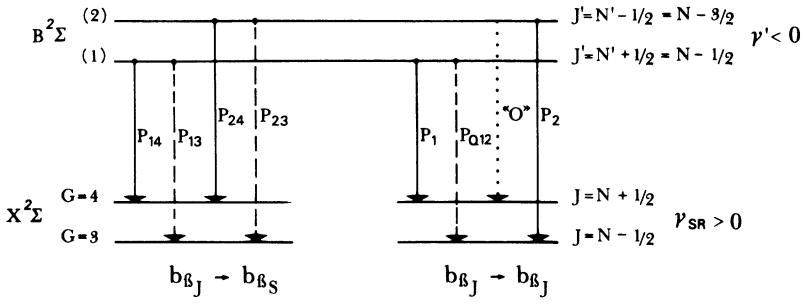

FIG. 6. Qualitative correlation between $^2\Sigma(b_{\beta J}) \rightarrow {}^2\Sigma(b_{\beta S} - b_{\beta J})$ transition. It should be noted that, in the pure $b_{\beta J} \rightarrow b_{\beta J}$ limit, P_{24} would become an "O" branch, the intensity of which is zero ($\Delta N = -2$).

an order of magnitude of these constants.

Moreover, the total intensities corresponding to each branch $J' \rightarrow G$ are given by [Eq. (B4) of the Appendix]

$$I_{J' \rightarrow G} = \sum_{F'F} I_{F'F} = \frac{(2J'+1)(2G+1)}{(2N'+1)(2S+1)} I_0(N', N) .$$

This expression leads to a constant value $\frac{9}{7}$ for the intensity ratios ρ_1 and ρ_2 of $G=4$ or $G=3$ components, although observed ratios are not constant with N (see Fig. 4). Then formulation in pure coupling appears insufficient to explain quite satisfactorily the experimental results.

C. Intermediate-Coupling Calculations

In Sec. III B, only the diagonal part in G of the Hamiltonian has been taken into account to deduce the expression of W_F as a function of the corresponding parameters of the ground state.

As the off-diagonal spin-rotation matrix elements between $G=3$ and $G=4$ states increase with N, a $b_{\beta J}$ tendency will appear for the $X^2\Sigma$ state: the coupling between $\vec{N}$ and $\vec{S}$ grows stronger with N, while it diminishes between $\vec{I}$ and $\vec{S}$. This breakdown effect allows a qualitative explanation of the observed deviation of the intensity ratios from the pure coupling value $\frac{9}{7}$. When considering each "$b_{\beta S}$," G wave function as a linear combination of the two basic "$b_{\beta J}$" ($J = N \pm \frac{1}{2}$) wave function [Eq. (B2)] connection can be established between pure $b_{\beta J} \rightarrow b_{\beta S}$ and pure $b_{\beta J} \rightarrow b_{\beta J}$ transitions. Let us suppose for instance, that γ_{SR} is positive, then, as N is increasing, the basic wave function $J = N + \frac{1}{2}$ becomes predominant in the $G=4$ state, while it is the $J = N - \frac{1}{2}$ for $G=3$; consequently the P_{14}, P_{13}, P_{23} transitions are shown to become, in the pure $b_{\beta J} \rightarrow b_{\beta J}$ limit, respectively, the P_1, P_{Q12}, P_2 transitions[29] while the P_{24} vanishes (Fig. 6), and then with increasing N, $\rho_1 \rightarrow \infty$ (P_1/P_{Q12}) while $\rho_2 \rightarrow 0$("O"$/P_2$).

This decoupling tendency explains qualitatively the observed variation with N of the intensity ratios and has now to be investigated quantitatively.

1. Energy Levels

The new energy levels W_F of the $X^2\Sigma$ states for each value of F are obtained by diagonalizing the matrix of the Fermi and spin-rotation Hamiltonian between $G=3$ and $G=4$ states, i.e.,

$$W_F = \tfrac{1}{2}(H_{33} + H_{44}) \pm \tfrac{1}{2}[(H_{33} - H_{44})^2 + 4H_{34}^2]^{1/2} , \qquad (7)$$

where $H_{33} = W_{G=3}(F)$, $H_{44} = W_{G=4}(F)$ and [Eq. (A2) of the Appendix]

$$H_{34} = \tfrac{1}{16}\gamma_{SR}[(F+N+5)(-F+N+4)(F-N+4)(F+N-3)]^{1/2} .$$

Each of the corresponding wave functions is a linear combination of the two pure coupling $b_{\beta S}$ wave functions $|G=3, FM_F\rangle$ and $|G=4, FM_F\rangle$ and can be written in a simplified way by introducing an effective breakdown coupling parameter ϵ. Indeed ϵ depends on F:

$$\begin{aligned} \psi_3(FM_F) &= (1-\epsilon^2)^{1/2}|G=3, FM_F\rangle - \epsilon|G=4, FM_F\rangle , \\ \psi_4(FM_F) &= +\epsilon|G=3, FM_F\rangle + (1-\epsilon^2)^{1/2}|G=4, FM_F\rangle . \end{aligned} \qquad (8)$$

In order to set up the theoretical spectra, we need also to express the corresponding intensities in intermediate coupling.

2. Intensities

The intensities are obtained from the dipolar electric momentum matrix elements between each sublevel of $B^2\Sigma$ in pure $b_{\beta J}$ coupling and each sublevel of $X^2\Sigma$ in intermediate coupling:

$$I(J'F' \rightarrow gF) = \sum_{\psi_F M'_F} \left| \langle (B^2\Sigma) J'F'M'_F | \sum_i \vec{r}_i | (X^2\Sigma)\psi_g(FM_F) \rangle \right|^2$$

Using the expressions (8) of $\psi_g(FM_F)$ one gets

$$I(J'F' \to g=3,F) = (1-\epsilon^2)I(J'F' \to G=3,F) + \epsilon^2 I(J'F' \to G=4,F) + 2\epsilon(1-\epsilon^2)^{1/2} \times (\pm)[I(J'F' \to G=3,F)I(J'F' \to G=4,F)]^{1/2},$$
$$I(J'F' \to g=4,F) = \epsilon^2 I(J'F' \to G=3,F) + (1-\epsilon^2)I(J'F' \to G=4,F) - 2\epsilon(1-\epsilon^2)^{1/2} \times (\pm)[I(J'F' \to G=3,F)I(J'F' \to G=4,F)]^{1/2}, \quad (9)$$

where the signs (±) are related to the values of J'; i.e., (+) stands for the level 2 ($J' = N' - \frac{1}{2}$) while (−) for the level 1 ($J' = N' + \frac{1}{2}$).

It should be noted, by disregarding in a first approximation the F dependence of ϵ, that it is easy to point out qualitatively the effect of breakdown of coupling on the intensity ratios. Indeed from Eq. (9) one obtains

$$\rho_1 = \frac{I(1 \to g=4)}{I(1 \to g=3)} = \frac{I(1 \to G=4) + 2\epsilon[I(1 \to G=3)I(1 \to G=4)]^{1/2}}{I(1 \to G=3) - 2\epsilon[I(1 \to G=3)I(1 \to G=4)]^{1/2}} > \frac{9}{7},$$

$$\rho_2 = \frac{I(2 \to g=4)}{I(2 \to g=3)} = \frac{I(2 \to G=4) - 2\epsilon[I(2 \to G=3)I(2 \to G=4)]^{1/2}}{I(2 \to G=3) + 2\epsilon[I(2 \to G=3)I(2 \to G=4)]^{1/2}} < \frac{9}{7}.$$

The matrix element H_{34} (and consequently ϵ) is an increasing function of N, and then the approximate expressions illustrate how the more ϵ (hence N) increases, the more the ratio deviates from $\frac{9}{7}$. To introduce quantitatively the effect of the breakdown coupling on the theoretical spectral lines, the values of ϵ are determined numerically by diagonalizing the energy matrix for each value of F. Some results are given in Table I to illustrate in a shortened way the true variation of ϵ with N and F, as well as the corresponding evolution of the ratios ρ_1 and ρ_2.

3. *Determination of the Constants*

Experimental values of the linewidths, which vary with N in a more appreciable way than the separation between the components, are used to obtain values of the fine and hyperfine constants. Nevertheless, to save computational time, approximate values of these constants are first deduced from the separations and then used as a starting point for the calculation.

TABLE I. Variations of ϵ with N and F and influence on the intensity ratios.

N		2	5	10	20	30	50
ϵ	$F = N-3$		0.003	0.008	0.018	0.028	0.050
	$F = N$	0.002	0.007	0.014	0.028	0.042	0.071
	$F = N+3$	0.003	0.006	0.010	0.019	0.028	0.044
ρ_1		1.30	1.32	1.35	1.47	1.6	1.8
ρ_2		1.27	1.24	1.20	1.10	1.05	0.92

In order to set up the theoretical rotational line shape, we first have to consider a single hyperfine experimental line (see Sec. II), the profile of which is picked up point by point. Then, a normalization, smoothing and interpolation program is used to reproduce it with an accuracy of 0.1 mK. From the knowledge of the theoretical values of the energies W_F and $W_{F'}$, [Eq. (7)], all the components of the resultant rotational line are positioned with regard to one of them with the same accuracy. The theoretical value of its intensity is attributed to each hyperfine component; the required rotational line shape then results from the composition of all these partial hyperfine components. The summation is performed every 4 mK.[30]

The approximate pure coupling values of the b, b', c', γ_{SR} parameters used as a starting point enable us to calculate values of intermediate-coupling energy levels W_F and $W_{F'}$ as well as the corresponding intensities $I_{FF'}$ [Eq. (9)].

Then the half-widths are determined by linear interpolation and compared to the experimental values. As small variations of b have no effect on the line shape, it appears sufficient to use the previously calculated value of b. The final value of the three parameters b', c', γ_{SR} are obtained by minimizing the standard deviation.

One gets for the $B^2\Sigma$ state

$$b' = 21.7 \pm 2.0 \text{ mK},$$

$$c' = -5 \pm 12 \text{ mK},$$

and for $X^2\Sigma$

$$\gamma_{SR} = 2.57 \pm 0.25 \text{ mK}.$$

The aforementioned error corresponds to a variation of the constant, which doubles the minimum standard deviation (=1.5 mK), when the other constants are fixed. The Fermi constant b of the $X^2\Sigma$ state is then obtained from the distance between the centers of gravity using the above-calculated values of b', c', and γ_{SR}.

One gets $b = 123.5 \pm 1.8$ mK. All these calculations have been performed on a CDC 6600 computer using programs specially written for this purpose.

IV. DISCUSSION

Theoretical variations with N of half-widths and distances between the centers of gravity of the lines are shown to be mainly in good agreement with the experimental results (see Figs. 2, 3, 7). Some discrepancies appear for small values of N ($N < 10$). Nevertheless, owing to their weak intensity, their overlapping and blending with the R branches, the experimental measures of the corresponding lines are not sufficiently accurate to justify the need of a more complete theoretical formulation. Calculation has been performed with and also without including the quadrupolar interaction. The comparison of the results shows how, when introducing this interaction, one gets better agreement, i.e., a significant decreasing of standard error allowing the determination of c'. Nevertheless, only an order of magnitude of c' is obtained, owing to the fact that it is mainly determined from data related to the first lines. The aforementioned values involve a Fermi contribution in b', which is seen to be about 20 ± 6 mK and can be attributed to small mixing of pure s-type orbitals in the $p\sigma$ of the $B\,^2\Sigma$ state.[31]

It is also noteworthy that the usual direct determination of the value of the Fermi constant b of the $X\,^2\Sigma$ state from the mean observed distance between the components of a line would lead to $4b = 465$ mK. The corresponding systematic error of about -30 mK arises mainly from neglecting the other interactions in the determination of the center of gravity of the lines.

For great values of N, the two groups of components, $\Delta F = 0$ and $\Delta F = +1$, vanish owing to the usual selection rule $\Delta N = -1 \rightarrow \Delta F = -1$.

In Fig. 7 experimental and theoretical profiles are compared qualitatively. The results concern $P_1(25)$ and $P_2(30)$ for which the components are sufficiently closed and not superposed. Similar shapes are observed for other lines with N greater than 10. The shapes are different for the lesser values of N, as the $\Delta F = 0, \pm 1$ components are not at all negligible.

Finally, it has been shown that the simplified theoretical scheme accounts for the principal features of the spectra and allows the determination of some constants, such as the value of b' in the excited state which, at the present time, is not yet attainable by classical methods. It should be noted how intensity studies may be a useful way to show a slight uncoupling.

ACKNOWLEDGMENT

We are particularly indebted to Dr. H. Lefebvre-Brion for many stimulating and useful discussions and for critically reading our manuscript.

APPENDIX A: HAMILTONIAN MATRIX ELEMENTS

In our calculations of matrix elements between $^2\Sigma$ states, we have only considered the nuclear part of spin-orbit operator, i.e.,[32]

$$\mathcal{H}_{SR} = 2g\mu_B^2 m \sum_K \frac{Z_K}{M_K} \sum_{i=1}^{N} \frac{1}{r_{iK}^3} (\vec{r}_{iK} \times \vec{p}_K) \vec{s}_i .$$

The hyperfine-structure Hamiltonian includes the Fermi contact term

$$\mathcal{H}_F = \zeta \frac{8\pi}{3} \sum_K \vec{\mu}_K \sum_i \delta(\vec{r}_{iK}) \vec{s}_i ;$$

the magnetic dipole-dipole interaction term

$$\mathcal{H}_D = \zeta \sum_K \vec{\mu}_K \cdot \sum_i \frac{1}{r_{iK}^3} \left(\vec{s}_i - \frac{3\vec{r}_{iK}(\vec{s}_i \cdot \vec{r}_{iK})}{r_{iK}^2} \right) ;$$

and the electric quadrupolar term

$$\mathcal{H}_Q = \frac{1}{\sqrt{5}} \left(\sum_K Q_K^2 \otimes \sum_i \frac{e_i}{r_{iK}^3} C^2(\theta_{iK}, \phi_{iK}) \right)^0 .$$

In these expressions $\vec{\mu}_K$ and Q_K^2 are, respectively, the magnetic dipole and electric quadrupolar moment operators of nucleus "K" and $\vec{s}_i$ the spin of electron "i." It should be noted that the hyper-

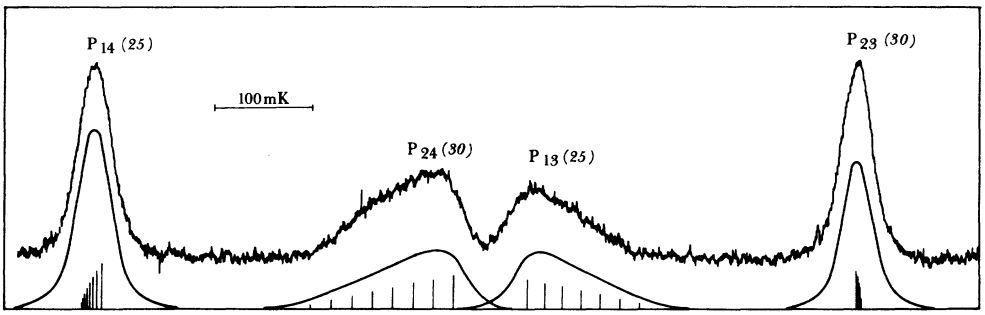

FIG. 7. Comparison of experimental and theoretical line shapes.

fine orbital term leads to vanishing matrix elements between Σ states ($\Lambda = 0$). The nuclear spin rotation interaction has been neglected. Now we have to express the matrix elements of these operators in b_{β_S} and in b_{β_J} coupling cases.[33]

1. Basic Wave Functions

The angular momentums are coupled in the following order: in the b_{β_S} coupling case,

$$\vec{N} = \vec{L} + \vec{R}, \quad \vec{G} = \vec{I} + \vec{S}, \quad \vec{F} = \vec{N} + \vec{G};$$

in the b_{β_J} coupling case,

$$\vec{N} = \vec{L} + \vec{R}, \quad \vec{J} = \vec{N} + \vec{S}, \quad \vec{F} = \vec{J} + \vec{I},$$

where $\vec{L}$, $\vec{R}$, $\vec{S}$, $\vec{I}$ are, respectively, the total electronic orbital momentum, the nuclear rotational angular momentum, the total electronic spin, and the nuclear spin momentums. The corresponding basic wave functions are, in the two cases,

$$|v\Lambda NM_N\rangle = \left(\frac{2N+1}{8\pi^2}\right)^{1/2} \mathfrak{D}^N_{\Lambda M_N}(\phi, \theta, 0)\psi_{v\Lambda}(\vec{r}_i, \vec{r}_{AB}),$$

where $\mathfrak{D}^N_{\Lambda M_N}(\phi, \theta, 0)$ are the well-known matrix elements of finite rotations particularized for diatomic molecules (degenerated axis), and M_N stands for the z component of $\vec{N}$ in the laboratory system. The total wave function, i.e., in b_{β_S} coupling $|\Lambda N(IS)GFM_F\rangle$ and in b_{β_J} coupling $|\Lambda(NS)JIFM_F\rangle$, may be derived by applying the usual coupling rules in the laboratory axis. As we use relationships of tensorial algebra, explicit formulation of these wave functions is not needed.

To calculate matrix elements of the different terms of the Hamiltonian and to show their dependence with N, we have introduced the following tensorial expression and effective parameters for the different interactions.

2. Effective Hamiltonians

Effective Hamiltonians with the usual approximation,[32] the tensorial form of the electronic spin–nuclear-orbit Hamiltonian is

$$\mathcal{H}_{SR} = \gamma_{SR}[T^1(S) \cdot T^1(N)],$$

where

$$\gamma_{SR} \sim \langle \Lambda | 2g\mu_B^2 m \sum_{K,i} \frac{Z_K}{M_K r_{iK}^3} | \Lambda \rangle$$

and $T^k(\ )$ stands for a tensor of rank k.[34]

In the case of b_{β_J} coupling, the hyperfine-structure Hamiltonian has been expressed in the general form

$$\mathcal{H}_{\text{hfs}} \sim \{T^{k_I}(I) \otimes \{T^{k_s}(s) \otimes T^{k_L}(L)\}^{k_I}\}^0$$

with for the magnetic terms $k_I = 1$ [$T^1(I) = \vec{\mu}$] and, respectively,

$$k_s = 1, \quad k_L = 0$$

for the Fermi contact term $\mathcal{H}_F$,

$$k_s = 2, \quad k_L = 2$$

for the dipole-dipole interaction $\mathcal{H}_D$, and with $k_I = 2$ for the electric quadrupolar term [$T^2(I) = Q$, $k_s = 0$, $k_L = 2$].

In the case of b_{β_S} coupling, we rather use the equivalent form obtained by the recoupling of angular momentums $\vec{I}$ and $\vec{S}$[35]:

$$\mathcal{H}_{\text{hfs}} \sim (-)^{k_L + k_S}(2k_I + 1)^{1/2}\{T^{k_L}(L) \otimes \{T^{k_I}(I) \otimes T^{k_s}(s)\}^{k_L}\}^0.$$

We can also note that these unified formulas are valid for the neglected terms. The evaluation of matrix elements is easy as far as the tensor operators act in the same system, i.e., the laboratory. Matrix elements of the tensor operators operating in the molecular frame are evaluated by a projection procedure.

3. Projection Procedure

By a classical tensorial calculation of the former terms in b_{β_J} or b_{β_S} coupling, we have to evaluate the following matrix elements:

$$\langle \Lambda' N' M'_N | T^{k_L}_q(L) | \Lambda N M_N \rangle .$$

The component q of the tensor $T^{k_L}(L)$ in the laboratory is deduced from its components m in the molecular frame as follows:

$$T^{k_L}_q(L) = \sum_m \mathfrak{D}^{k_L}_{mq}(\phi, \theta, 0) T^{k_L}_m(L);$$

so one gets [see Ref. 34, Eq. (4-6-2)]

$$\langle \Lambda' N' M'_N | T^{k_L}_q(L) | \Lambda N M_N \rangle = \frac{[(2N+1)(2N'+1)]^{1/2}}{8\pi^2} \langle \Lambda' \mathfrak{D}^{N'}_{\Lambda' M'_N} | \sum_m \mathfrak{D}^{k_L}_{mq} T^{k_L}_q(L) | \Lambda \mathfrak{D}^N_{\Lambda M_N} \rangle$$

$$= (-)^{\Lambda' - M'_N}[(2N+1)(2N'+1)]^{1/2} \begin{pmatrix} N' & k_L & N \\ -M'_N & q & M_N \end{pmatrix} \begin{pmatrix} N' & k_L & N \\ -\Lambda' & \Lambda' - \Lambda & \Lambda \end{pmatrix} \langle \Lambda' | T^{k_L}_{\Lambda' - \Lambda}(L) | \Lambda \rangle .$$

This procedure involves the calculation of an electronic integral which will be taken as a parameter.

4. Matrix Elements

In the case of b_{β_S} coupling, the hyperfine matrix elements are

$$\langle \Lambda' N'(IS')G'F'M'_F | \mathcal{H}_{\rm hfs} | \Lambda N(IS)GFM_F\rangle = (-)^{N+G'+F+k_S+N'-\Lambda'}(2k_I+1)^{1/2}\delta_{FF'}\delta_{M'_F M_F}[(2G+1)(2G'+1)(2N+1)(2N'+1)]^{1/2}$$
$$\times \begin{Bmatrix} N' & N & k_L \\ G & G' & F \end{Bmatrix} \begin{Bmatrix} I & I & k_I \\ S' & S & k_S \\ G' & G & k_L \end{Bmatrix} \begin{pmatrix} N' & k_L & N \\ -\Lambda' & q & \Lambda \end{pmatrix}$$
$$\times \langle I \| T^{k_I}(I) \| I \rangle \langle S' \| T^{k_S}(S) \| S \rangle \langle \Lambda' | T^{k_L}_q(L) | \Lambda \rangle . \tag{A1}$$

The spin–nuclear-orbit term is evaluated in a same way:

$$\langle b'_{\beta_S} | \mathcal{H}_{SR} | b_{\beta_S} \rangle = \gamma_{SR}(-)^{N+G'+F+S'+I+G+1}\delta_{FF'}\delta_{M_F M'_F}\delta_{NN'}[(2G+1)(2G'+1)]^{1/2}$$
$$\times \begin{Bmatrix} F & G' & N' \\ 1 & N & G \end{Bmatrix} \begin{Bmatrix} S' & G' & I \\ G & S & 1 \end{Bmatrix} [N(N+1)(2N+1)]^{1/2} \langle S' \| T^1(S) \| S \rangle . \tag{A2}$$

A similar calculation for the b_{β_J} case gives

$$\langle \Lambda' N' S' J' I F' M'_F | \mathcal{H}_{\rm hfs} | \Lambda N S J I F M_F \rangle = \langle b'_{\beta_J} | \mathcal{H}_{\rm hfs} | b_{\beta_J} \rangle = (-)^{F+N'-\Lambda'+J+I}\delta_{FF'}\delta_{M_F M'_F}\delta_{II'}(2k_I+1)^{1/2}$$
$$\times [(2J+1)(2J'+1)(2N+1)(2N'+1)]^{1/2} \begin{Bmatrix} J' & J & k_I \\ I & I & F \end{Bmatrix} \begin{Bmatrix} N' & N & k_L \\ S' & S & k_S \\ J' & J & k_I \end{Bmatrix} \begin{pmatrix} N' & k_L & N \\ -\Lambda' & q & \Lambda \end{pmatrix}$$
$$\times \langle I \| T^{k_I}(I) \| I \rangle \langle S' \| T^{k_S}(S) \| S \rangle \langle \Lambda' | T^{k_L}_q(L) | \Lambda \rangle \tag{A3}$$

and

$$\langle b'_{\beta_J} | \mathcal{H}_{SR} | b_{\beta_J} \rangle = (-)^{N+S'+J}\delta_{FF'}\delta_{M_F M'_F}\delta_{JJ'} \begin{Bmatrix} N' & N & 1 \\ S & S' & J \end{Bmatrix} [N(N+1)(2N+1)]^{1/2} \langle S' \| T^1(S) \| S \rangle . \tag{A4}$$

APPENDIX B: INTENSITIES

The electric dipolar momentum matrix elements for a transition $b_{\beta_J} \to b_{\beta_J}$ is

$$\langle \Lambda' N' S' J' I F' M'_F | \sum_i r_i | \Lambda N S J I F M_F \rangle \sim \langle \Lambda' N' S' J' I F' M'_F | T^1_q(L) | \Lambda N S J I F M_F \rangle = A_{J'F'M'_F \to JFM_F}$$
$$= (-)^{F'+F+J'+J+I+S'-M'_F-\Lambda'}[(2F+1)(2F'+1)(2J+1)(2J'+1)(2N+1)(2N'+1)]^{1/2}$$
$$\times \begin{pmatrix} F' & 1 & F \\ -M'_F & q & M_F \end{pmatrix} \begin{Bmatrix} J' & F' & I \\ F & J & 1 \end{Bmatrix} \begin{pmatrix} N' & 1 & N \\ -\Lambda' & \Lambda'-\Lambda & \Lambda \end{pmatrix} \langle \Lambda' | T^1_{\Lambda'-\Lambda}(L) | \Lambda \rangle .$$

Therefore the total intensity of each branch is

$$I_{J' \to J} \sim \sum_{q M_F M'_F} \sum_{F F'} |A_{J'F'M'_F JFM_F}|^2 = (2I+1)(2J+1)(2J'+1) \begin{Bmatrix} N' & J' & S \\ J & N & 1 \end{Bmatrix}^2 (2N+1)(2N'+1)$$
$$\times \begin{pmatrix} N' & 1 & N \\ -\Lambda' & \Lambda'-\Lambda & \Lambda \end{pmatrix}^2 |\langle \Lambda' | T^1_{\Lambda'-\Lambda}(L) | \Lambda \rangle|^2 , \tag{B1}$$

which gives the usual dependence with J of Mulliken formulas.[36]

The intensities between b_{β_S} and b_{β_J} states are obtained by expressing the b_{β_S} wave function in terms of b_{β_J} wave functions, i.e.,

$$|\Lambda N(IS)GFM_F\rangle = (-)^{F+I+S+N}(2G+1)^{1/2} \sum_J (2J+1)^{1/2} \begin{Bmatrix} F & I & J \\ S & N & G \end{Bmatrix} |\Lambda (NS)JIFM_F\rangle . \tag{B2}$$

So, the matrix elements for $b_{\beta_J} \to b_{\beta_S}$ transitions are

$$\langle \Lambda'(N'S')J'IF'M'_F | T^1_q(L) | \Lambda N(IS)GFM_F \rangle = A_{J'F'M'_F \to GFM_F} = (-)^{2F'-M'_F+G+F+1-\Lambda'+N'+S'+I}$$
$$\times [(2F+1)(2F'+1)(2G+1)(2J'+1)(2N+1)(2N'+1)]^{1/2}$$
$$\times \begin{pmatrix} F' & 1 & F \\ -M'_F & q & M_F \end{pmatrix} \begin{Bmatrix} F' & N' & G' \\ F & N & 1 \end{Bmatrix} \begin{Bmatrix} F' & N' & J' \\ I & F' & G \end{Bmatrix} \begin{pmatrix} N' & 1 & N \\ -\Lambda' & \Lambda'-\Lambda & \Lambda \end{pmatrix}$$
$$\times \langle \Lambda' | T^1_{\Lambda'-\Lambda}(L) | \Lambda \rangle .$$

Then, the intensity of a hyperfine component is

$$I_{J'F'\to GF} = \sum_{q M_F M_F'} |A_{J'F'M_F'\to GFM_F}|^2 = (2F'+1)(2F+1)\begin{Bmatrix} N' & F' & G \\ F & N & 1 \end{Bmatrix}^2 \begin{Bmatrix} N' & S' & J' \\ I & F' & G \end{Bmatrix}^2 (2G+1)(2J'+1)(2N'+1)(2N+1)$$
$$\times \begin{pmatrix} N' & 1 & N \\ -\Lambda' & \Lambda'-\Lambda & \Lambda \end{pmatrix}^2 |\langle \Lambda' | T^1_{\Lambda'-\Lambda}(L) | \Lambda \rangle|^2 . \tag{B3}$$

Finally, the total intensity of each branch is

$$I_{J'\to G} = \sum_{FF'} I_{J'F'\to GF} = \frac{(2G+1)(2J'+1)(2N+1)}{2S'+1} \begin{pmatrix} N' & 1 & N \\ -\Lambda' & \Lambda'-\Lambda & \Lambda \end{pmatrix}^2 |\langle \Lambda' | T^1_{\Lambda'-\Lambda}(L) | \Lambda \rangle|^2 . \tag{B4}$$

---

[1]L. Åkerlind, Ark. Fys. 22, 65 (1962).
[2]P. Carette and J. Blondeau, C. R. Acad. Sci. B 268, 1743 (1969).
[3]D. W. Green, Can. J. Phys. 49, 2552 (1971).
[4]L. Åkerlind, Ark. Fys. 22, 41 (1962).
[5]A. Adams, W. Klemperer, and T. M. Dunn, Can. J. Phys. 46, 2213 (1968).
[6]C. Athenour, R. Bacis, J. L. Femenias, and R. Stringat, C. R. Acad. Sci. B 271, 567 (1970).
[7]R. Stringat, C. Athenour, and J. L. Femenias, Can. J. Phys. 50, 395 (1972).
[8]M. Marcano and R. F. Barrow, J. Phys. B 3, 2121 (1970).
[9]C. B. Suarez, J. Phys. B 3, 1389 (1970).
[10]R. Bacis, A. Bernard, and J. d'Incan, C. R. Acad. Sci. B 273, 272 (1971).
[11]R. Bacis and A. Bernard, Can. J. Phys. 51, 648 (1973).
[12]L. Brewer and R. M. Walsh, J. Chem. Phys. 42, 4055 (1965).
[13]K. D. Carlson, E. Ludena, and C. Moser, J. Chem. Phys. 43, 2408 (1965).
[14]R. A. Berg, L. Wharton, W. Klemperer, A. Buchler, and J. L. Stauffer, J. Chem. Phys. 43, 2416 (1965).
[15]W. Weltner, D. McLeod, Jr., and P. H. Kasai, J. Chem. Phys. 46, 3172 (1967).
[16]T. M. Dunn, *Molecular Spectroscopy, Modern Research* (Academic, New York, 1972), p. 231.
[17]R. Bacis, C. R. Acad. Sci. B 266, 1071 (1968).
[18]R. Bacis (unpublished).
[19]R. Chabbal and P. Jacquinot, Rev. Opt. Theor. Instrum. 4, 157 (1961).
[20]A. Giachetti, R. W. Stanley, and R. Zalubas, J. Opt. Soc. Am. 60, 474 (1970).
[21]R. Bacis, Appl. Opt. 10, 535 (1971).
[22]J. H. Van Vleck, Phys. Rev. 33, 467 (1929).
[23]T. M. Dunn, XIII colloque spectr. Int. Ottawa 1967 (Hilger, London, 1968), p. 363.
[24]D. W. Green, J. Phys. Chem. 75, 3103 (1971).
[25]I. Kovacs, *Rotational Structure in the Spectra of Diatomic Molecules* (Hilger, London, 1969).
[26]*Nuclear Data Tables*, edited by K. Way (Academic, New York, 1969).
[27]W. J. Childs and L. S. Goodman, Phys. Rev. A 1, 25 (1971).
[28]For b' and c' Townes and Schawlow's notations (Ref. 33) are used.
[29]Herzberg's notation is used for these transitions (Ref. 36).
[30]One does not get a significant change of the results by using smaller spacing.
[31]It is well known that the hyperfine contribution of a s orbital is usually much greater than a p one of the same shell.
[32]K. Freed, J. Chem. Phys. 45, 4214 (1966).
[33]C. H. Townes and A. L. Schawlow, *Microwave Spectroscopy* (McGraw-Hill, New York, 1955).
[34]A. R. Edmonds, *Angular Momentum in Quantum Mechanics* (Princeton U. P., Princeton, N. J., 1957).
[35]B. R. Judd, *Operator Techniques in Atomic Spectroscopy* (McGraw-Hill, New York, 1963).
[36]G. Herzberg, *Molecular Spectra and Molecular Structure* (Van Nostrand, New York, 1967), Vol. I.